JACS
JOURNAL OF THE AMERICAN CHEMICAL SOCIETY
Article
pubs.acs.org/JACS

Oxyanion Hole Stabilization by C−H···O Interaction in a Transition State—A Three-Point Interaction Model for *Cinchona* Alkaloid-Catalyzed Asymmetric Methanolysis of *meso*-Cyclic Anhydrides

Hui Yang and Ming Wah Wong*

Department of Chemistry, National University of Singapore, 3 Science Drive 3, Singapore 117543

Supporting Information

ABSTRACT: Oxyanion holes are commonly found in many enzyme structures. They are crucial for the stabilization of high-energy oxyanion intermediates or transition states through hydrogen bonding. Typical functionalities found in enzyme oxyanion holes or chemically designed oxyanion-hole mimics are N−H and O−H groups. Through DFT calculations, we show that asymmetric methanolysis of *meso*-cyclic anhydrides (AMMA) catalyzed by a class of *cinchona* alkaloid catalysts involves an oxyanion hole consisting of purely C−H functionality. This C−H oxyanion hole is found to play a pivotal role for stabilizing the developing oxyanion, via C−H···O hydrogen bonds, in our newly proposed three-point interaction transition-state model for AMMA reactions, and is the key reason for the catalyst to adopt the *gauche*-open conformation in the transition state. Predicted enantioselectivities of three *cinchona* alkaloid catalysts, namely DHQD-PHN, DHQD-MEQ, and DHQD-CLB, based on calculations of our transition-state model, agree well with experimental findings.

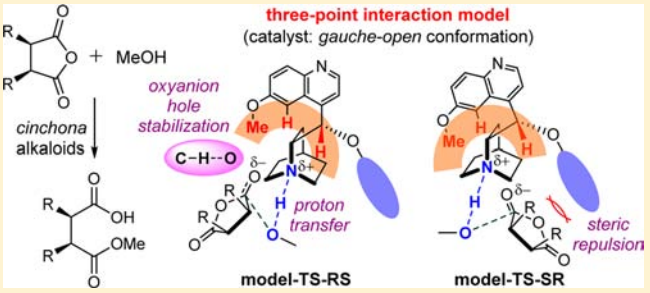

INTRODUCTION

Oxyanions are ubiquitous in chemistry and biology and are important intermediates in many biological important reactions; for example, the tetrahedral intermediate in peptide hydrolysis by serine protease is an oxyanion.[1] The term "oxyanion hole" has been coined to describe a mechanism of stabilization of transition states involving oxyanions by a pocket structure in enzymes that can bind favorably to the oxyanions.[2] Previous studies have shown that the functional groups in the hole that are responsible for the binding are typically N−H or O−H, e.g., in the active site of serine protease (Scheme 1).

Scheme 1. Oxyanion Hole in the Active Site of Serine Protease

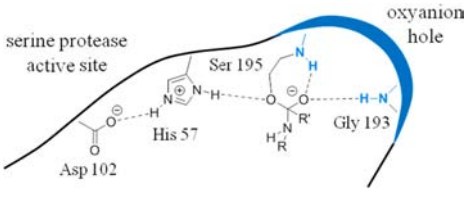

Strong hydrogen bonds are formed between these groups and the oxyanion. Such a concept has inspired many beautiful design works in chemistry, mimicking a pocket-like structure with either designed enzymes (theozymes) or small organic molecules.[3]

It is well established that C−H···O interactions[4] exist in small-molecule crystal[5] and protein structures.[6] The hydrogen-bond nature of this type of intermolecular force is widely accepted.[7] These weak C−H···O hydrogen bonds play an important role in the supramolecular chemistry, crystal engineering, structures, and functions of biological macromolecules and stabilization of transition states. Through a solid-state and quantum mechanical study, C−H···O interaction is shown to be a determinant of molecular conformation.[8] C−H···O has similarly been reported to be a controlling factor in supramolecular complex.[9] Quite recently, a colorimetric anion-sensing system was developed, based on multiple C−H···O hydrogen bonds.[10] In organocatalysis, the important role of C−H···O hydrogen bonds has been elegantly demonstrated experimentally and computationally.[11] We envisaged that an oxyanion could be stabilized by C−H···O hydrogen bonds alone. For negatively charged oxygen atoms, the C−H···O interaction energy is substantially larger than that in neutral oxygen atoms. For instance, the calculated binding energy of $CH_4\cdots OH^-$ is −24.5 kJ/mol (CCSD(T)/aug-cc-pVTZ+BSSE), 10 times greater than that of the corresponding neutral complex $CH_4\cdots OH_2$, −2.5 kJ/mol. In fact, the magnitude of the binding energy is comparable to that of a typical hydrogen bond, e.g., in water dimer. Hence, a C−H functional group could be used in an oxyanion hole to stabilize transition states with a developing oxyanion.

Received: January 18, 2013
Published: March 21, 2013

   dx.doi.org/10.1021/ja4005893 | *J. Am. Chem. Soc.* 2013, 135, 5808−5818

Among the many organic reactions that involve an oxyanion as either an intermediate or a transition state, asymmetric methanolysis of *meso*-cyclic anhydrides (AMMA) catalyzed by *cinchona* alkaloids represents a facile pathway to build functionalized organic molecules with multiple stereogenic centers.[12−15] It was shown in a series of elegant studies that the methanolysis reaction proceeds via a general base-catalyzed mechanism (Scheme 2).[14,15] Proton transfer from methanol to

Scheme 2. Asymmetric Methanolysis of *meso*-Cyclic Anhydride and Proposed General Base Mechanism[a]

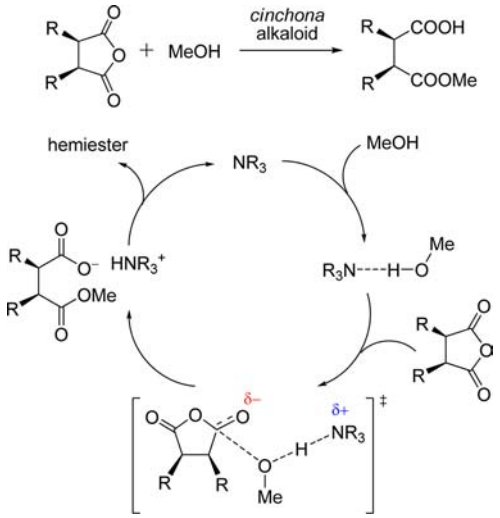

[a]NR_3 represents a *cinchona* alkaloid catalyst.

the tertiary nitrogen of the quinuclidine moiety of the catalyst and formation of C−O bond between methanol and the anhydride take place simultaneously in the rate-determining step. Thus, an oxyanion is developing in the transition state. Similar to the oxyanion hole found in enzymes, many *cinchona* alkaloid catalysts incorporate N−H or O−H functionality to stabilize and orient the developing oxyanion.[16] High levels of enantioselectivity (>90% ee) could be achieved using this strategy. A summary of a number of these *cinchona* alkaloid catalysts is presented in Scheme 3.

Scheme 3. *Cinchona* Alkaloid Catalysts That Incorporate N−H or O−H Functional Group(s)

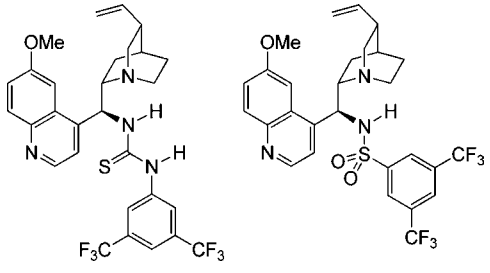

It is intriguing to note that Deng et al. reported a class of *cinchona* catalysts for AMMA reactions in 2000,[14a] which had been employed as chiral ligands in the Sharpless asymmetric dihydroxylation reaction.[17] Some of them yielded enantiomeric excess (ee) of greater than 90% for AMMA reaction of 2,3-dimethylsuccinic anhydride. One of the salient features of these catalysts is the lack of any hydrogen bond donor functionalities (Scheme 4). A recent study by the same group hypothesized a transition-state model based on simple steric reasoning.[14b]

Scheme 4. *Cinchona* Catalysts Lacking a N−H or O−H Functionality

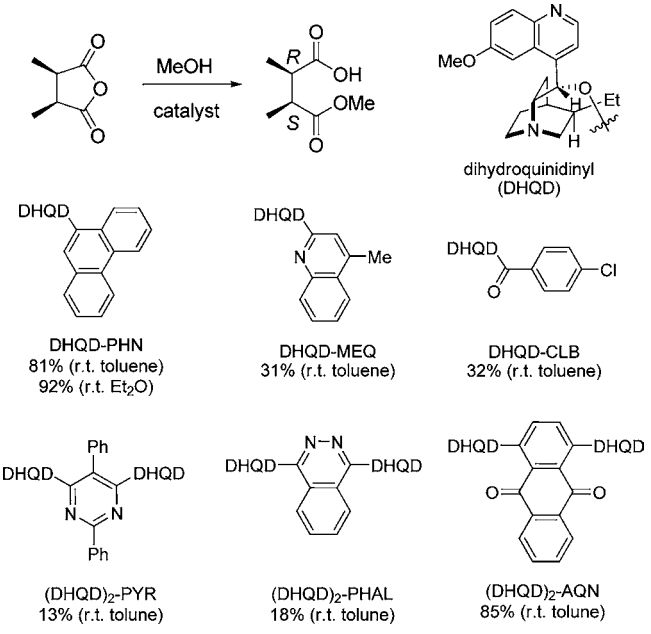

These authors suggested that the high level of enantioselectivity can be attributed to the bulky substituted group which helps to differentiate the catalyst conformation in the transition state. A low-cost catalyst was synthesized and demonstrated to be similarly effective, based on the prediction of their transition-state model.[14b]

The other major finding of Deng's study is the elucidation of the active conformation of *cinchona* catalysts, i.e., the conformation which controls the reaction stereoselectivity. Earlier studies have indicated that the catalysts can adopt four major conformations in solution, namely *app*-closed, *app*-open, *gauche*-closed, and *gauche*-open (Scheme 5).[18] This makes

Scheme 5. Four Key Conformations of *Cinchona* Alkaloids

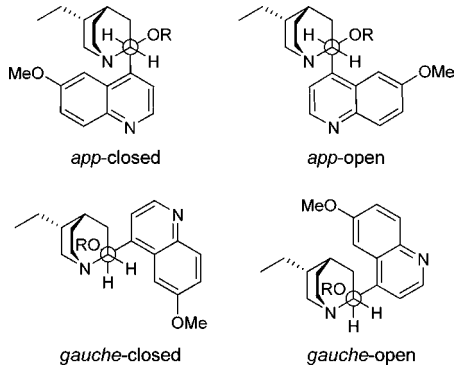

analysis of stereoselective *cinchona* alkaloid-catalyzed reactions significantly more complex and has led to confusion in the literature as to which conformer is the active conformation. The *gauche*-open conformation has been proposed to be the active conformation for asymmetric Michael reactions,[19] Diels−Alder reactions,[20] and Henry reactions,[21] while the *app*-closed conformation was proposed by Deng et al. to be the active

dx.doi.org/10.1021/ja4005893 | J. Am. Chem. Soc. 2013, 135, 5808−5818

conformation for AMMA reactions catalyzed by DHQD-PHN (Scheme 4).[14b]

Despite the significant progress made by Deng and others, a clear understanding of the transition-state structures for AMMA reactions catalyzed by *cinchona* alkaloids, as shown in Scheme 2, is still lacking. In particular, it is not known whether the developing oxyanion is stabilized by the catalyst. For the anhydride substrate in AMMA reactions, it can interact with the *cinchona* catalyst via multiple C−H···O hydrogen bonds. We postulate that multiple C−H hydrogens of the catalyst may form an oxyanion hole to stabilize transition states with a developing negatively charged oxygen atom. For a better mechanistic understanding of the *cinchona* alkaloid-catalyzed AMMA reactions, three fundamental questions need to be addressed: (1) whether the developing oxyanion is stabilized in the transition state for this class of catalysts via C−H···O oxyanion hole; (2) how the two possible enantiomeric oxyanions are differentiated in the transition state; and (3) which is the active conformation and what is the key reason for adopting the active conformation. Computational chemistry can provide crucial structural insights into transition states, which are still not accessible by experimental means to date. To this end, computational studies of AMMA reactions catalyzed by Deng's *cinchona* catalysts were carried out to shed light on these important issues.

■ COMPUTATIONAL METHODS

Geometry optimizations were performed with M06-2X[22] density functional theory and the standard 6-31G* basis set. This level of theory makes optimizations of transition states with full *cinchona* catalysts, e.g., DHQD-PHN (95 atoms), affordable, and it has been shown that it is adequate for organocatalyzed reactions.[23] Weak intermolecular interactions, such as C−H···π and C−H···O, are expected to be important in the transition states studied here. Thus, a more vigorous theoretical treatment of longer range interactions, such as the M06-2X method,[24,25] is essential for this computational study. Frequency analyses were performed on the M06-2X/6-31G* optimized geometries to confirm the nature of the stationary points as equilibrium structures (with all real frequencies) or transition states (with only one imaginary frequency). Higher level single-point energy calculations were performed at the M06-2X/6-311+G** level. Solvation free energies were evaluated at the M06-2X/6-31G* level of theory with Truhlar's SMD[26] method with toluene used as a solvent. Natural bond orbital (NBO) analysis was carried out at the M06-2X/6-31G* level to study the charge distribution and donor−acceptor interactions.[27] Charge density analysis, based on Bader's theory of atoms in molecules (AIM),[28] was carried out using the MORPHY98 program.[29] For the $CH_4\cdots OH^-$ and $CH_4\cdots OH_2$ complexes, their binding energies were calculated at CCSD(T)/aug-cc-pVTZ level, including basis set superposition error (BSSE) via the counterpoise method.[30] Unless otherwise noted, the relative energies reported in the text correspond to relative enthalpies (ΔH) and free energies (ΔG) at 298 K, computed at the M06-2X/6-311+G**//M06-2X/6-31G* level. Zero-point energy, temperature, and entropy corrections were obtained at the M06-2X/6-31G* level. All calculations were performed with the Gaussian 09 software package.[31]

■ RESULTS AND DISCUSSION

Conformations of DHQD-PHN. As outlined in the Introduction, one of the most confusing issues about *cinchona* catalysts is their active conformation. Particularly for the catalysts examined in this study, the 6′-methoxy group of the quinoline moiety (Scheme 4) was found to be important for high enantioselectivity.[14b] Thus, a systematic conformational analysis, including an analysis of the 6′-methoxy group, was carried out initially to shed light on this vital issue. *Cinchona* catalysts are rigid molecules containing relatively few rotatable bonds. Torsional angles around rotatable single bonds in the vicinity of the two chiral carbon atoms, namely C8 and C9 (Scheme 6), are crucial structural parameters of the conformational space of *cinchona* catalysts. Four torsional angles were identified for DHQD-PHN (Scheme 4) and labeled as α (∠N1−C8−C9−C4′), β (∠C8−C9−C4′−C3′), γ (∠C8−C9−O10−C9″), and δ (∠C9−O10−C9″−C10″) (Scheme 6). It is well established that the quinuclidine moiety of *cinchona* catalysts is asymmetrically twisted. For instance, an NMR study by Sharpless et al. showed that the quinuclidine moiety of DHQD-CLB is right-handed, twisted at about 20°.[18a] Hence, the quinuclidine ring twist is also treated in this study as an asymmetric feature of *cinchona* catalysts. Here, we define a parameter ε as the torsional angle ∠N1−C8−C7−C4 (Scheme 6). Optimized structural parameters of the four conformations of DHQD-PHN are given in Figure 1.

Scheme 6. Numbering and Definition of Torsional Angles α−ε of the Three *Cinchona* Alkaloid Catalysts Examined in This Study

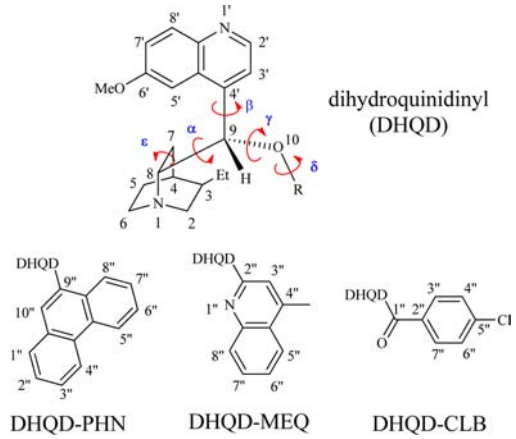

Our calculated results indicate that the 6′-methoxy group of the quinoline moiety is coplanar to the quinoline ring, and the preferred conformation of the methyl group is *trans* to C7′ of quinoline; e.g., for *app*-closed-PHN, a *cis*-coplanar structure of the 6′-methoxy group is 14.1 kJ/mol higher in energy than the preferred *trans*-coplanar structure. This calculated structural feature agrees well with experimentally reported crystal structures of several natural *cinchona* alkaloids.[32] All four conformations of DHQD-PHN are close in energy, with the *gauche*-open conformation slightly more stable than the other three (Figure 1). In accordance with the experimental finding, all four conformations are right-hand twisted. With respect to the effect of the $-O_{10}R$ substituent on the conformational distribution, only a short contact due to C−H···π interaction between the quinoline moiety's 6′-methoxy group and one of the rings of phenanthrene is observed in *app*-open and *gauche*-closed but not in *app*-closed or *gauche*-open conformations, as shown in Figure 1.

Based on our conformational analysis result, there is no distinct active conformation of DHQD-PHN. Thus, it seems unlikely that the catalyst adopts a dominant conformation in solution which single-handedly gives rise to the observed ee. In other words, it is essential to consider all four conformations in transition states of the crucial C−O bond-forming step in order

dx.doi.org/10.1021/ja4005893 | J. Am. Chem. Soc. 2013, 135, 5808−5818

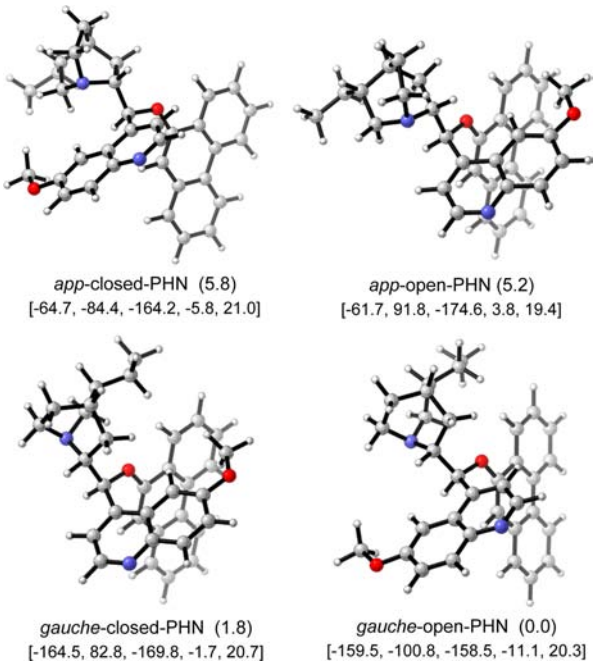

Figure 1. Optimized (M06-2X/6-31G*) geometries of four conformers of DHQD-PHN. Calculated relative energies (ΔH, kJ/mol) are given in parentheses. Values of torsional angles (α, β, γ, δ, and ε, in degrees) are given in square brackets.

to elucidate the active conformation and origin of enantioselectivity. It is important to note that a kinetic study of isotope effects on methanol's hydroxyl proton strongly suggests that the rate-determining step is the C−O bond-forming step, as shown in Scheme 2.[14b]

Model Catalysts. A systematic conformational study of all possible transition states of AMMA catalyzed by *cinchona* catalysts such as DHQ-PHN is very resource-demanding. Instead, a simple scheme was formulated to extrapolate results of smaller model systems so as to minimize the need to calculate all possible transition states with a full catalyst (Scheme 6). The first step of our devised scheme is to study an achiral tertiary amine, trimethylamine (TMA), as a catalyst for the model AMMA reaction (Scheme 8). A systematic search of the conformational space of transition states was performed to elucidate the plausible important interactions in the C−O bond-forming transition states. Next, chiral induction by *cinchona* catalysts was considered by investigating two chiral quinuclidines, 3,8-dimethylquinuclidine (DMQC) and DQHD-Ph (Scheme 7).

To reveal the origin of high enantioselectivity for DHQD-PHN, key transition states with the full DHQD-PHN structure were located, based on extrapolation of the result of DHQD-

Scheme 7. Model Catalysts for AMMA Reactions in This Study

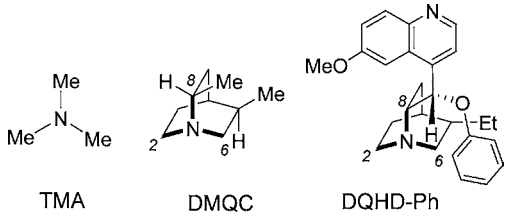

Scheme 8. Model Reaction of TMA-Catalyzed Methanolysis of Succinic Anhydride

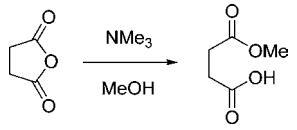

Ph. Finally, the role of $-O_{10}R$ substituents was also examined. Two similar DHQD derivatives which give low enantioselectivities, namely DHQD-MEQ and DHQD-CLB, were compared to the computational result of DHQD-PHN.

Trimethylamine-Catalyzed Methanolysis of Cyclic Anhydride. Based on the key finding of various kinetic studies,[14,15] we assumed in this study that proton transfer from methanol to TMA and formation of a C−O bond between methanol and anhydride take place simultaneously; in other words, it involves a concerted transition state. This is confirmed by examining a plausible stepwise mechanism, i.e., proton transfer followed by C−O bond formation in two steps. In particular, we searched for the formation of an ion-pair complex via proton transfer from methanol to TMA. An extensive search via scanning the potential energy surface indicates that a protonated TMA-methoxy ion-pair complex does not exist. A similar result was obtained for proton transfer between quinuclidine and methanol. It is worth noting that Bolm et al. have proposed an alternate catalytic pathway which involves an attack of the anhydride by the more nucleophilic alkaloid nitrogen.[13] However, a recent computational study by Dedeoglu et al. has shown that this alternate pathway is more than 100 kJ/mol higher in energy than the general base-catalyzed mechanism.[15b]

For the concerted transition state, six possible transition states (**I**–**VI**) with a staggered conformation around the forming C−O bond were identified (Scheme 9). Three out of

Scheme 9. Six Possible C−O Bond-Forming Transition States of TMA-Catalyzed AMMA Reaction

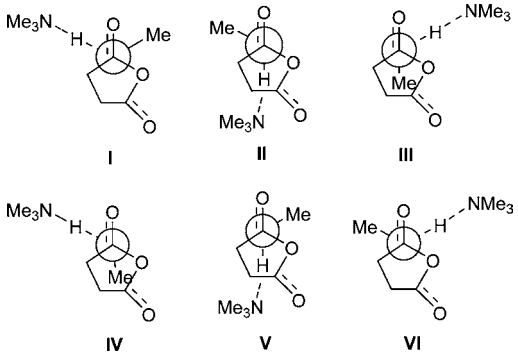

the six transition-state conformations were successfully located, namely **I**, **III**, and **VI**. The relative energies are 26.3, 11.5, and 0.0 kJ/mol respectively. **I** and **VI** are both expected to experience less steric interaction as compared to **III**. The calculated large energy difference between **I** and **VI** and relatively small energy difference between **III** and **VI** suggest that the developing oxyanion is substantially stabilized in both **III** and **VI**. The propensity of the anhydride oxygen atoms in close contact with the catalyst in transition states is clearly a result of maximizing the electrostatic interaction between the developing negative charge in oxygen atoms and the developing

dx.doi.org/10.1021/ja4005893 | J. Am. Chem. Soc. 2013, 135, 5808−5818

positive charge in the catalyst. Thus, only transition states of conformation type **VI** were considered subsequently for the larger catalysts.

Next, we explored plausible conformations of the reacting methanol−anhydride complex with respect to the catalyst in conformation **VI**. A relaxed potential energy surface scan was performed as follows. Key structural parameters were frozen at the values of **VI**, namely the forming C−O bond at 1.701 Å, O−H at 1.410 Å, and N−H at 1.141 Å. Two torsional angles ϕ and θ were defined as coordinates of the conformational space of **VI** (Figure 2). ϕ is confined between 0 and 120° so that the

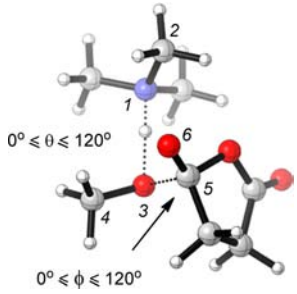

Figure 2. Definition of torsional angles θ (∠C4−O3−N1−C2) and ϕ (∠O6−C5−O3−C4) for the transition state of TMA-catalyzed AMMA reaction. The atomic labels 1−6 are used only in this diagram for the definition of the two angles.

conformational space examined will be limited to the vicinity of **VI**. Due to the C_3 symmetry of TMA, θ is only scanned from 0 to 120°. Two energy minima were located, one at $\theta \approx 30°$, $\phi \approx 60°$ and the other at $\theta \approx 90°$, $\phi \approx 50°$ (see Figure S1 in Supporting Information). The latter is the global minimum of the potential energy surface and corresponds to the original transition state **VI**. Full geometry optimization of the first local energy minimum leads to a new transition-state conformation, with similar bonding parameters (forming C−O bond at 1.715 Å, O−H at 1.399 Å, and N−H at 1.149 Å). To distinguish the two conformations of transition state **VI** (**TS-TMA-VI**), we defined the first as **VIA** and the second **VIB** (Figure 3). Both transition states are stabilized by multiple C−H···O hydrogen bonds, with the interaction distance ranging from 2.32 to 2.56 Å. Based on NBO second-order perturbation theory analysis, the total stabilization energies amount to 16.9 and 20.6 kJ/mol for **VIA** and **VIB**, respectively (Figure 3). **VIB** is calculated to be 4.5 kJ/mol higher in energy than **VIA**. This is probably due to the smaller ϕ value calculated for **VIA**, which permits a closer electrostatic interaction between the anhydride oxygen atoms and the catalyst. The calculated activation enthalpy of transition state **VIA** with respect to the pre-transition-state complex is 65.5 kJ/mol ($\Delta G^{\ddagger}_{298}$ = 82.6 kJ/mol).

Dimethylquinuclidine-Catalyzed Methanolysis Reaction. Dimethylquinuclidine (DMQC, Scheme 7) possesses the same stereochemistry at C3 and C8 as DHQD and derivatives but has no substituent on the C8-methyl group (Scheme 6). This makes DMQC an ideal model to understand the origin of enantioselectivities of DHQD-derived *cinchona* catalysts. Unlike the C_3-symmetric TMA, DMQC does not have a C_3 rotation axis. The three α carbon atoms are distinguishable. According to our definition of θ as shown in Figure 2, and the conformational study of transition states as shown in Figure S1, it is possible to define four values of θ for each α carbon, at $\theta \approx$ 30, 90, −30, and −90°, respectively. In total, 12 transition

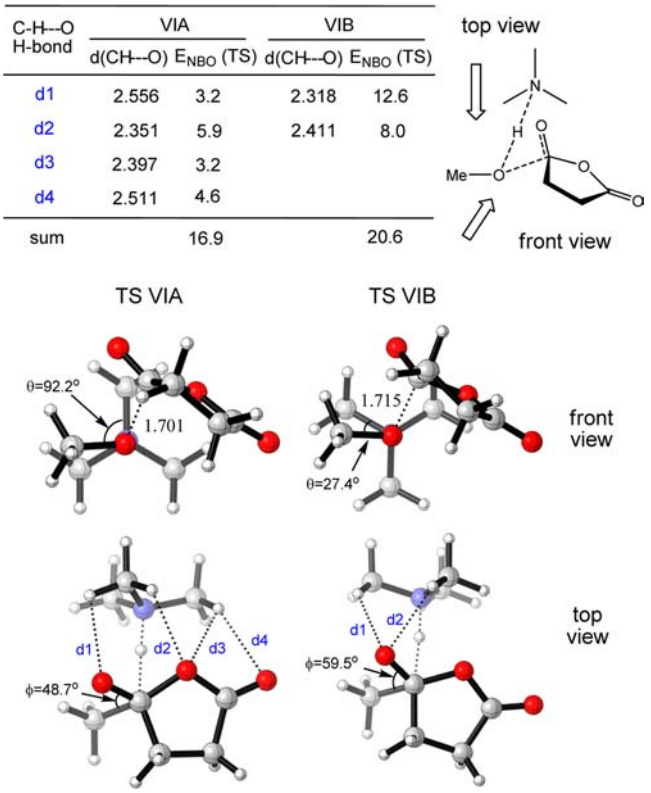

Figure 3. Optimized (M06-2X/6-31G*) geometries of the two conformations of **TS-TMA-VI**, **VIA** and **VIB**, in front view (left) and top view (right). C−H···O distances in Å and NBO interaction energies in kJ/mol.

states are anticipated. The same model reaction as shown in Scheme 8 was studied to search for the 12 possible transition states. The calculated relative energies and structural parameters of the successfully located transition states are presented in Table 1.

Table 1. Calculated Relative Energies[a] ($\Delta\Delta H^{\ddagger}$ and $\Delta\Delta G^{\ddagger}$, kJ/mol) for Various Transition States Located for DMQC-Catalyzed Methanolysis Reaction

transition state	θ/°	C$^{\alpha}$	$\Delta\Delta H^{\ddagger}$	$\Delta\Delta G^{\ddagger}$
TS-DMQC-1	−81.9	C8	3.6	1.4
TS-DMQC-2	−52.3	C8	8.3	7.7
TS-DMQC-3	22.8	C8	9.1	6.2
TS-DMQC-4	72.6	C8	9.3	6.4
TS-DMQC-5	−73.9	C6	2.9	3.7
TS-DMQC-6	−8.0	C6	3.8	2.7
TS-DMQC-7	88.8	C6	0.0	0.0
TS-DMQC-8	25.8	C2	3.8	5.5
TS-DMQC-9	110.2	C2	8.3	8.7

[a]M06-2X/6-311+G**//M06-2X/6-31G* level.

It is instructive to examine the results in Table 1 in greater detail. As shown in Figure 2, θ is defined with an α carbon atom in such a manner that methanol and anhydride are reacting in its vicinity. C6 of DMQC, which is the furthest α carbon away from the C8-methyl group, defines transition states with the lowest energies, i.e., **TS-DMQC-5**, **-6**, and **-7**. Only one other transition state, **TS-DMQC-1**, defined with C8, is comparable in energy. The optimized structure of **TS-DMQC-1** is shown in

dx.doi.org/10.1021/ja4005893 | J. Am. Chem. Soc. 2013, 135, 5808−5818

Figure 4. A very short C−H···O hydrogen bond between the C8-methyl group and the oxygen atom of the attacked

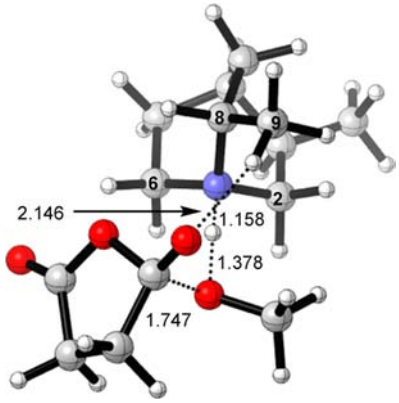

Figure 4. Optimized (M06-2X/6-31G*) geometry of transition state **TS-DMQC-1**. Bond distances in Å.

carbonyl, with O···H distance measured at 2.146 Å and CHO angle at 161.8°, is observed for **TS-DMQC-1**. NBO analysis indicates that this C−H···O interaction is characterized by a large stabilization energy of 23.0 kJ/mol, which is close to the binding energy of the prototypical CH_4···OH^- complex (−24.0 kJ/mol) and is attributed to the developing negative charge of the oxygen atom (NBO charge = −0.73 e). The short C9−H···O contact is partly due to this large stabilization energy and partly due to the rather rigid N···H···O(CH_3)···C−O structural framework arising from simultaneous proton transfer and C−O bond formation in the transition state. These computational results clearly indicate that a single C−H···O interaction to the C9-methyl group of DMQC can substantially stabilize the developing oxyanion. Hence, for more complex *cinchona* alkaloid catalysts, even when they do not contain a classical hydrogen bond donor such as a hydroxyl group, it is still necessary to consider those transition states that permit multiple nonclassical C−H···O hydrogen bonds to anhydride, in addition to those transition states with least steric hindrance. This is especially important for *cinchona*-catalyzed reactions operating a general base mechanism, when deprotonation of substrates by *cinchona* catalysts generates electron-rich oxyanion intermediates and/or transition states that permit stronger C−H···O interaction. For this reason, in subsequent studies, we examined not only transition states defined with C6 but also transition states analogous to **TS-DMQC-1**.

Due to the C−H···O interaction and the developing anion character in the transition states, diffuse and polarization functions are expected to be important. Thus, we have performed additional geometry optimizations of **TS-DMQC-1**, the transition state with a very strong C−H···O hydrogen bond, and **TS-DMQC-7**, the lowest energy transition state, at the M06-2X/6-31+G** level. However, compared to the 6-31G* optimized geometries, the structural changes are insignificant. We then carried out M06-2X/6-311+G** single-point energy calculations at the M06-2X/6-31+G** optimized geometries. The computed relative energy of **TS-DMQC-1** with respect to **TS-DMQC-7** using the M06-2X/6-31+G** geometries is 3.9 kJ/mol, only 0.1 kJ/mol different from the value of 4.0 kJ/mol based on the 6-31G* geometries. This suggests that the use of the 6-31G* basis set in geometry optimizations is adequate. Finally, we have also performed MP2/6-311+G** single-point energy calculations on **TS-DMQC-1** and **TS-DMQC-7**. The calculated relative energy (3.5 kJ/mol) is in close agreement with the DFT value (3.9 kJ/mol). This lends confidence to our choice of the M06-2X functional in energy prediction.

DHQD-Ph-Catalyzed Methanolysis Reaction. Next, we examined DHQD-Ph-catalyzed methanolysis reaction to elucidate the active conformation. A thorough search for transition states analogous to **TS-DMQC-1**, **-5**, **-6**, and -7 with all four conformations of DHQD-Ph was carried out. The analogue of **TS-DMQC-1** is defined as having an optimal θ value of −90° with respect to C8 (Table 1). Other transition states are defined in the same manner. Methanolysis of dimethylsuccinic anhydride (Scheme 4) was studied. For disubstituted anhydrides, there are two possible modes of attack to the methanol-catalyst complex, leading to two types of transition states, namely MA1 and MA2 (Scheme 10). Due to steric repulsion between the R′ and methyl groups, transition states of MA2 type are generally expected to be higher in energy relative to their corresponding MA1 transition states. Hence, MA1 transition states were studied initially, key transition states were identified, and their corresponding MA2 transition states were then examined. It should be noted that MA1 transition states with negative θ values will lead to (2*R*,3*S*)-hemiacetal, the major product observed for DHQD-PHN catalyst. The computational results are summarized in entries 1−16 of Table 2.

Scheme 10. Two Possible Conformers of Transition State for AMMA Reactions with a Disubstituted *meso*-Cyclic Succinic Anhydride

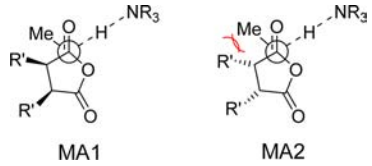

Our calculated results in entries 1−13 of Table 2 indicate that the *gauche*-open conformation derived transition states are generally much lower in energy than the others. This disagrees with the literature proposal of the *app*-closed conformation as the active conformation, although entries 1−4 in Table 2 also predict the (2*R*,3*S*)-hemiacetal is preferred if the *app*-closed conformation is the active conformation. Having shown the *app*-closed and *gauche*-open conformations are close in energy, it is intriguing to ask what is the origin of the large energy difference between the C−O bond-forming transition states originating from different conformations. Close examination of the structures of *gauche*-open derived transition states indicates the presence of an oxyanion hole in the catalyst. It helps to stabilize the anhydride substrate in the transition state.

To better understand the structural requirement on the *cinchona* catalysts and to estimate the strength of stabilization, a more detailed investigation of the oxyanion hole in the relevant transition states was carried out. The oxyanion hole for the major transition state **TS-Ph-RS8** consists of three C−H hydrogens, namely C9−H_3, C5′−H_2, and 6′-methoxy H_1. These hydrogens stabilize the developing oxyanion via C−H···O hydrogen bonds, with C−H···O distances from the hydrogens to the oxygen of the attacked carbonyl group measured at 2.16−2.56 Å (Figure 5). These C−H···O distances are all significantly shorter than the sum (2.72 Å) of the van der Waals radii of hydrogen and oxygen atoms. In particular, the

dx.doi.org/10.1021/ja4005893 | *J. Am. Chem. Soc.* 2013, 135, 5808−5818

Table 2. Relative Energies[a] ($\Delta\Delta H^{\ddagger}$ and $\Delta\Delta G^{\ddagger}$, kJ/mol) and Structural Parameters of Various Transition States of DHQD-Ph-Catalyzed Methanolysis Reaction

entry	transition state	$\Delta\Delta H^{\ddagger}$	$\Delta\Delta G^{\ddagger}$	C_{α}	mode	θ	conformation
1	**TS-Ph-RS1**	32.0	37.8	C6	MA1	−66.2	*app*-closed
2	**TS-Ph-RS2**	37.6	43.2	C6	MA1	−44.8	*app*-closed
3	**TS-Ph-SR1**	44.8	47.9	C6	MA1	+111.6	*app*-closed
4	**TS-Ph-RS3**	70.8	71.2	C8	MA1	−71.9	*app*-closed
5	**TS-Ph-RS4**	34.1	36.6	C6	MA1	−37.5	*app*-open
6	**TS-Ph-SR2**	41.6	47.1	C6	MA1	+107.5	*app*-open
7	**TS-Ph-RS5**	56.0	48.6	C6	MA1	−70.5	*gauche*-closed
8	**TS-Ph-RS6**	45.9	45.7	C6	MA1	−32.6	*gauche*-closed
9	**TS-Ph-SR3**	30.0	28.9	C6	MA1	+101.4	*gauche*-closed
10	**TS-Ph-RS7**	21.7	16.2	C8	MA1	−86.9	*gauche*-closed
11	**TS-Ph-SR4**	17.2	17.0	C6	MA1	+94.5	*gauche*-open
12	**TS-Ph-RS8**	0.0	0.0	C8	MA1	−78.5	*gauche*-open
13	**TS-Ph-SR5**	14.4	18.0	C8	MA1	+81.2	*gauche*-open
14	**TS-Ph-RS9**	28.5	33.4	C6	MA2	+106.1	*gauche*-open
15	**TS-Ph-SR6**	6.3	10.2	C8	MA2	−73.6	*gauche*-open
16	**TS-Ph-RS10**	20.3	25.8	C8	MA2	+66.3	*gauche*-open

[a]M06-2X/6-311+G**//M06-2X/6-31G* level.

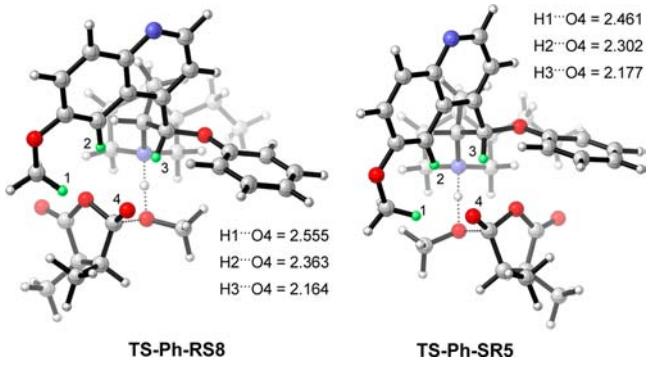

Figure 5. Optimized (M06-2X/6-31G*) geometries of **TS-Ph-RS8** and **TS-Ph-SR5**. H1−H3 are the hydrogen atoms of the oxyanion hole. C−H···O distances in Å.

rather short distance (2.16 Å) and almost linear CHO angle (170.9°) between the C9−H_3 and the anhydride oxygen suggest an important role of this C−H···O interaction, which is not attainable in the *app* type of conformation (Scheme 5). NBO charge density analysis shows that the positive charge on the C9 hydrogen is as large as that on the α-carbon hydrogens (Figure S2). To provide a quantitative estimation of the interaction strength of these C−H···O hydrogen bonds, NBO second-order perturbation analysis at the M06-2X/6-31G* level was performed. It gives a stabilization energy of 27.3 kJ/mol for the C9−H···O hydrogen bond (Figure 6). Similarly, interaction energies of the other two C−H···O hydrogen bonds of the binding pocket are estimated to be 11.1 and 5.2 kJ/mol for C5′-H_2 and 6′-methoxy H_1, respectively. The magnitude of stabilization energy correlates well with the C−H···O interaction distance. Thus, the C9−H_3 is the main source of oxyanion hole stabilization. The combined stabilization energy of the C−H oxyanion hole, 43.6 kJ/mol, can readily rival that of a classical hydrogen bond (10−30 kJ/mol). This oxyanion hole stabilization leads to a greatly decreased activation enthalpy of 34.7 kJ/mol ($\Delta G^{\ddagger}_{298}$ = 46.5 kJ/mol), as compared to 65.5 kJ/mol ($\Delta G^{\ddagger}_{298}$ = 82.6 kJ/mol) for the TMA catalyst. The pivotal role of stabilization by the oxyanion hole is also manifested in the fact that the calculated lowest energy transition state, **TS-Ph-RS8**, is defined with the sterically congested C8 instead of C6 (Scheme 6).

The hydrogen bond nature of C−H···O interactions in the oxyanion hole is further supported by examining the topological properties of electron density using Bader's AIM theory.[28] The C−H···O interactions in **TS-Ph-RS8** show correct charge density topology for a typical hydrogen bond.[7c] There exists a bond path and its associated bond critical point (bcp) between the interacting C−H hydrogen and oxygen atom. The signs and magnitudes of the charge density (ρ) and Laplacian of the charge density ($\nabla^2\rho$) evaluated at the bcp's (Figure 7) are similar to those of the intermolecular C−H···O and C−H···N hydrogen-bonded systems.[7c,33] It is worth noting that the stronger C−H···O hydrogen bond is reflected in

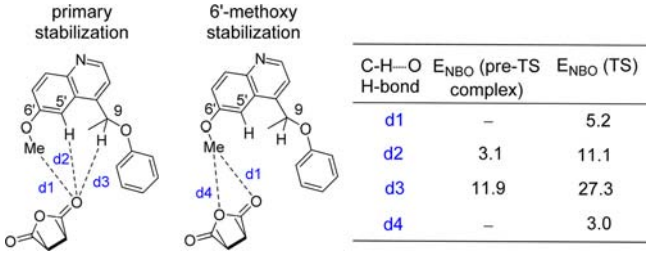

C-H···O H-bond	E_{NBO} (pre-TS complex)	E_{NBO} (TS)
d1	–	5.2
d2	3.1	11.1
d3	11.9	27.3
d4	–	3.0

Figure 6. NBO second-order perturbation energy analysis of C−H···O interactions in transition state **TS-Ph-RS8**. NBO interaction energies in kJ/mol.

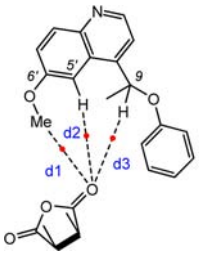

C-H···O H-bond	ρ	$\nabla^2\rho$
d1	0.0088	0.0303
d2	0.0129	0.0422
d3	0.0192	0.0586

Figure 7. Bond critical points (represented by dots) and topological properties (ρ and $\nabla^2\rho$) of the three C−H···O hydrogen bonds in **TS-Ph-RS8**.

dx.doi.org/10.1021/ja4005893 | J. Am. Chem. Soc. 2013, 135, 5808−5818

the larger ρ and $\nabla^2\rho$ values. In summary, the C−H···O interactions in the oxyanion hole exhibit the characteristic charge density topology of a typical weak hydrogen bond.

Secondary stabilization by the C−H hole is also observed for **TS-Ph-RS8**, as shown in Figure 6. The combined stabilization of the anhydride by the 6′-methoxy group amounts to 8.2 kJ/mol. Thus, our calculation suggests that the role of 6′-methoxyl group is attractive instead of repulsive as proposed by Deng et al.[14b] This agrees well with the experimental finding that removing the 6′-methoxy group from the catalyst leads to decreases in both reactivity and enantioselectivity.

In view of the vital stabilization role of the C−H oxyanion hole, we reviewed the extrapolation from catalyst DMQC to DQHD-Ph and calculated an analogue of **TS-DMQC-4**, **TS-Ph-SR5** in Figure 5, which can also maximize stabilization of the developing oxyanion by the C−H oxyanion hole (entry 13 of Table 2). The computed result suggests that it is another important transition state for the minor (2*S*,3*R*) product, with energy comparable to that of the original lowest-energy *SR* transition state, i.e., **TS-Ph-SR4**. This confirms the essential role of the C−H oxyanion hole in stabilizing transition-state structures with high-energy oxyanions and explains the large energy differences between *app*-closed and *gauche*-open derived transition states.

Our proposal that the *gauche*-open conformation might be the active conformation is supported by a recent NMR study by Balzano et al., who reported the tendency of *cinchona* catalysts to undergo *app*-to-*gauche* transitions in the presence of alcohols.[15c] An electrostatic potential map of the *gauche*-open conformation of DHQD-PHN clearly indicates the existence of a C−H oxyanion hole (Figure 8) and, hence, further validates our proposition.

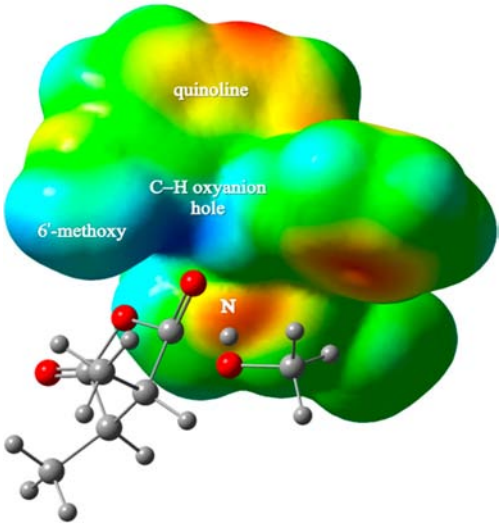

Figure 8. Electrostatic potential map of the *gauche*-open conformation of DHQD-PHN in transition state **TS-Ph-RS8**. Red indicates electron-rich region while blue represents electron-poor region.

Finally, we explored the MA2 type of transition states. Three MA1 transition states were identified as key transition states, namely **TS-Ph-RS8** for the major (2*R*,3*S*) product, and **TS-Ph-SR4** and **TS-Ph-SR5** for the minor (2*S*,3*R*) product. Their corresponding MA2 transition states, namely **TS-Ph-SR6**, **TS-Ph-RS9**, and **TS-Ph-SR10**, were calculated, and their relative energies are given in Table 2 (entries 14−16). **TS-Ph-SR6** was identified as the third key transition state for the (2*S*,3*R*) product. Overall, our computational results in Table 2 suggest the *gauche*-open conformation is the active conformation for AMMA reactions. The predicted major product for methanolysis of 2,3-dimethylsuccinic anhydride catalyzed by cinchona alkaloids catalyst, the (2*R*,3*S*)-hemiacetal, agrees well with the experimental result.[14]

Proposed Transition-State Model. Based on our calculated results of various model catalysts, we propose a transition-state model (**model-TS**, Scheme 11) applying a three-point interaction model to account for the stereoselectivity of AMMA reactions.[34] The key features of our model are the following: (1) The *gauche*-open conformation, whose quinuclidine nitrogen is most accessible to methanol and anhydride without much steric repulsion from the quinoline moiety, unlike the *app* type of conformation, and which possesses a C−H oxyanion hole, is the active conformation. (2) Proton transfer between the quinuclidine nitrogen and methanol is the primary point of interaction between the catalyst and substrates. (3) The oxyanion hole comprising multiple C−H bonds, via C−H···O interactions, is the second point of interaction. (4) The O_{10} substituent is the third point of interaction, via steric repulsion.

Scheme 11. Proposed New Transition-State Model (model-TS) Based on the *gauche*-Open Conformation for DHQD-Derived *Cinchona* Catalysts

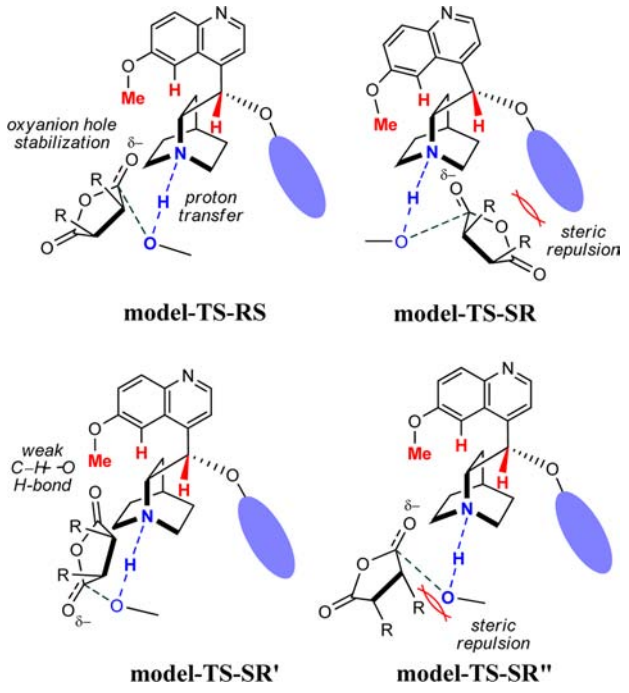

The most stable transition state predicted by our model, **model-TS-RS**, which is an analogue of **TS-Ph-RS8**, leads to the major (2*R*,3*S*) enantiomer. It maximizes attractive C−H···O interactions between the C−H oxyanion hole and the developing oxyanion and avoids steric repulsion exerted by the O_{10} substituent or methanol. For comparison, our model also predicts three higher energy transition states for the minor (2*S*,3*R*) enantiomer, namely **model-TS-SR** (an analogue of **TS-Ph-SR5**), **model-TS-SR′** (an analogue of **TS-Ph-SR4**), and **model-TS-SR″** (an analogue of **TS-Ph-SR6**). **Model-TS-SR** lacks a secondary C−H···O interaction to the ring oxygen of

dx.doi.org/10.1021/ja4005893 | *J. Am. Chem. Soc.* 2013, 135, 5808−5818

Table 3. Calculated Geometric Parameters and Relative Energies for Various Transition States of DHQD-PHN-, DHQD-MEQ-, and DHQD-CLB-Catalyzed Methanolysis Reactions[a]

transition state	$\Delta\Delta H^{\ddagger}$	$\Delta\Delta G^{\ddagger}$	$\Delta\Delta G^{\ddagger}_{sol}$	α	β	γ	δ	ε	θ
TS-PHN-RS	0.0	0.0	0.0	−176.0	−99.5	−161.7	+1.1	+22.2	−80.5
TS-PHN-SR	14.9	21.1	29.1	−161.5	−84.4	−146.9	−20.3	+20.4	+67.7
TS-PHN-SR′	11.6	16.0	20.3	−179.9	−104.1	−143.7	−13.8	+24.9	+94.9
TS-PHN-SR″	6.3	9.2	10.1	−176.2	−99.0	−165.0	+3.6	+21.5	−79.5
DHQD-PHN				−159.5	−100.8	−158.5	−11.1	+20.3	
TS-MEQ-RS	0.0	0.0	0.0	−176.0	−99.9	−162.7	−0.2	+19.9	−72.3
TS-MEQ-SR	3.0	13.6	23.4	−164.2	−96.7	−143.1	−22.8	+10.2	+78.3
TS-MEQ-SR′	7.0	12.3	16.5	+172.4	−104.9	−145.6	−7.2	+26.8	+94.6
TS-MEQ-SR″	7.8	11.3	11.5	−175.7	−99.6	−163.0	+0.1	+19.6	−73.1
DHQD-MEQ				−150.1	−104.1	−154.6	−5.4	+7.2	
TS-CLB-RS	0.0	0.0	0.0	−177.0	−99.4	−161.6	−1.9	+21.0	−72.4
TS-CLB-SR	7.7	8.2	11.6	−165.2	−95.2	−162.4	−8.6	+17.2	+86.1
TS-CLB-SR′	10.1	9.7	13.3	+164.6	−106.0	−136.4	−9.5	+26.2	+87.7
TS-CLB-SR″	8.4	11.3	12.2	−176.7	−99.5	−161.2	−2.4	+21.0	−73.6
DHQD-CLB				−164.5	−100.6	−156.4	−3.1	+19.7	

[a]M06-2X/6-311+G**//M06-2X/6-31G* level. Relative energies are given in kJ/mol and torsional angles in degrees.

anhydride and experiences steric repulsion from the O_{10} substituent; **model-TS-SR′** has only the weaker C−H···O stabilization involving a neutral oxygen atom, while **model-TS-SR″** experiences steric repulsion between anhydride substituents and methanol. It is important to note that alternate transition states leading to the (2*R*,3*S*) product are significantly higher in energy, based on the results of the DHQD-Ph-catalyzed methanolysis reaction (Table 2).

Next, we applied our proposed transition-state model to DHQD-PHN, which gives a high enantioselectivity of 81% in toluene at room temperature, and DHQD-MEQ and DHQD-CLB, which give equally low enantioselectivities of 30% in toluene at room temperature.[14a] Our calculated $\Delta\Delta H^{\ddagger}$ values for these three catalysts (Table 3) are in good accord with the experimental results, although for DHQD-CLB our results only qualitatively predict the right trend. Inclusion of solvent effect does not lead to significant changes in the trend of relative energies (Table 3). It is worth noting that DHQD-Ph models DHQD-PHN reasonably well with reduced computational cost. As seen in Tables 2 and 3, the computed relative energies of the two systems are in close agreement.

We observed that those catalysts that are not efficient for AMMA reactions, e.g., $(DHQD)_2$-PYDZ, are actually excellent chiral ligands for Sharpless dihydroxylation reaction. In the well-established Corey−Noe model of the transition-state complex of Sharpless dihydroxylation reaction,[35] the importance of pyridazine nitrogen in binding to alkene substrates, based on crystal structures of $(DHQD)_2$-PYDZ complexes, was pointed out by the authors as the key for the high efficiency of $(DHQD)_2$-PYDZ.[35b] This literature precedent, together with the observation of generally low levels of enantioselectivity for *cinchona* catalysts bearing heteroatom(s), nitrogen or oxygen, β to oxygen 10, led us to hypothesize that the low enantioselectivity is attributed to the β heteroatom. To lend support to our hypothesis, calculations of the nitrogen analogues of DHQD-Ph (**1**) and DHQD-PHN (**5**), and the carbon analogue of DHQD-MEQ (**4**), namely **2**, **6**, and **3**, respectively (Scheme 12), were carried out. Our results in Table 4 clearly show that the nitrogen substitution in catalysts **2**, **4**, and **6** leads to more favorable *SR* type of transition states and, hence, a lower level of enantioselectivity. The subtle difference can be explained using our transition-state model.

Scheme 12. Investigated *Cinchona* Alkaloid Catalysts (1−3) and Their Nitrogen Analogues (4−6) for AMMA Reactions

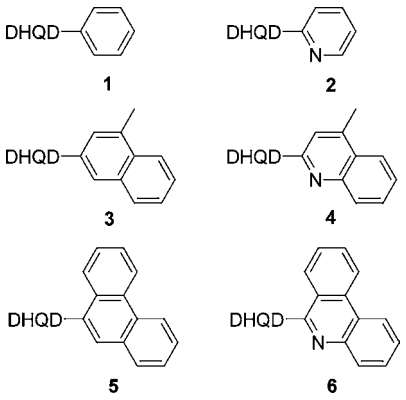

First, the heteroatom impedes the binding of anhydride to the oxyanion hole (Figure S3). Thus, the **model-TS-SR′** type of transition state is less unfavorable compared to the **model-TS-RS** type. Second, the substituted heteroatom withdraws electron density from the substituent's π system, rendering it less sterically repulsive, and reduces the energy difference between **model-TS-SR** and **model-TS-RS** types of transition states. This argument is supported by the well-known fact that pyridine is less prone to electrophilic substitution reactions than benzene.[36] In summary, our computational results in Table 4 suggest that transition states of **model-TS-SR** and **model-TS-SR′** are important to explain the low levels of enantioselectivity observed for DHQD-MEQ and DHQD-CLB.

Deng et al. have also proposed a stereochemical model to explain the observed asymmetric induction of AMMA reactions catalyzed by *cinchona* alkaloids.[14b] What are the differences between our TS model and Deng's model? First, Deng suggested the *app*-closed conformation to be the active conformation, while we proposed the *gauche*-open form. Second, the 6′-methoxy group of DHQD acts as a repulsive group in Deng's model, while it is part of the oxyanion hole via attractive C−H···O interactions in our model. Lastly, the developing oxyanion in the transition state is stabilized by the oxyanion hole in our proposed model; however, Deng did not consider the stabilization of the oxyanion.

dx.doi.org/10.1021/ja4005893 | J. Am. Chem. Soc. 2013, 135, 5808−5818

Table 4. Calculated Relative Energies[a] ($\Delta\Delta H^{\ddagger}$ and $\Delta\Delta G^{\ddagger}$, kJ/mol) for a Set of Test Catalysts Shown in Scheme 12

	model-TS-RS		model-TS-SR		model-TS-SR′		model-TS-SR″	
catalyst	$\Delta\Delta H^{\ddagger}$	$\Delta\Delta G^{\ddagger}$	$\Delta\Delta H^{\ddagger}$	$\Delta\Delta G^{\ddagger}$	$\Delta\Delta H^{\ddagger}$	$\Delta\Delta G^{\ddagger}$	$\Delta\Delta H^{\ddagger}$	$\Delta\Delta G^{\ddagger}$
1	0.0	0.0	14.4	18.0	17.2	17.0	6.3	10.2
2	0.0	0.0	7.9	10.9	13.1	14.4	7.9	10.7
3	0.0	0.0	10.7	18.9	11.3	14.4	6.7	10.8
4	0.0	0.0	3.0	13.6	7.0	12.3	7.8	11.3
5	0.0	0.0	14.9	21.1	11.6	16.0	6.3	9.2
6	0.0	0.0	6.4	12.9	7.2	9.6	7.4	9.8

[a]M06-2X/6-311+G**//M06-2X/6-31G* level.

CONCLUDING REMARKS

In conclusion, we have examined computationally the conformational space of the transition states of *cinchona* alkaloid-catalyzed AMMA reactions. We have found that in the C−O bond-forming transition states the developing oxyanion is stabilized and aligned by multiple C−H···O hydrogen bonds between the anhydride oxygens and the catalyst. A potential energy surface scan of the transition state for the TMA catalyst reveals two well-characterized conformations, **VIA** and **VIB**. These two conformations are found to be quite general and conserved in structure, as demonstrated by subsequent studies of other catalysts. Based on calculations of three model catalysts, namely TMA, DMQC, and DHQD-Ph, a three-point interaction transition-state model derived from the *gauche*-open conformation of *cinchona* alkaloid catalysts is proposed. This conformation is in contrast to the *app*-closed conformation proposed previously as the active conformation. An oxyanion hole comprising multiple C−H hydrogen bond donors in the *gauche-open* conformation was identified as the main reason for adopting the active conformation and the key factor for controlling enantioselectivity. Applying our new transition-state model to three *cinchona* alkaloid catalysts, the predicted enthalpy differences between transition states leading to the two enantiomeric products agree well with experimental data.

It should be emphasized that C−H···O interaction has long been recognized as a driving force of binding for many phase-transfer catalysis reactions by quaternary ammonium salts of cinchona alkaloids.[37] It is also well documented that C−H···O interaction is an important stereocontrol factor in Lewis acid-catalyzed organic reactions involving an aldehyde substrate.[38] However, its use in chiral recognition of oxyanions is still overlooked. Thus, it comes as no surprise that, in the seminal work of Deng and co-workers, their transition-state model was developed without application of any C−H···O interaction. To this end, we hope that the demonstrated ability of multiple C−H···O interactions to stabilize and align oxyanions in this paper may encourage researchers to exploit C−H···O interaction as a general protocol for future applications in organocatalysis, drug development, anion sensing, supramolecular chemistry, crystal engineering, and medicine.[8−11,39]

ASSOCIATED CONTENT

Supporting Information

Complete ref 31; total energies (Table S1) and Cartesian coordinates of all optimized structures (in .xyz format, zip file); relaxed potential energy surface scan of **TS-TMA-VI** (Figure S1); NBO charges of selected transitions states (Figure S2); and optimized transition-state geometries of DHQD-PHN, DHQD-MEQ, and DHQD-CLB catalysts (Figure S3). This material is available free of charge via the Internet at http://pubs.acs.org.

AUTHOR INFORMATION

Corresponding Author

chmwmw@nus.edu.sg

Notes

The authors declare no competing financial interest.

ACKNOWLEDGMENTS

This research was supported by the National University of Singapore (Grant No. R-143-000-481-112).

REFERENCES

(1) (a) Hayashi, Y.; Itoh, T.; Ohkubo, M.; Ishikawa, H. *Angew. Chem., Int. Ed.* **2008**, *47*, 4722. (b) Boyer, P. D. *Annu. Rev. Biochem.* **1997**, *66*, 717. (c) Hiroshi, F.; Zhang, X.; Tomita, T.; Ikeda-Saito, M.; Yoshida, T. *J. Am. Chem. Soc.* **2001**, *123*, 6475. (d) Suksai, C.; Tuntulani, T. *Chem. Soc. Rev.* **2003**, *32*, 192.

(2) (a) Sigala, P. A.; Kraut, D. A.; Caaveiro, J. M. M.; Pybus, B.; Ruben, E. A.; Ringe, D.; Petsko, G. A.; Herschlag, D. *J. Am. Chem. Soc.* **2008**, *130*, 13696. (b) Carrasco, N.; Hiller, D. A.; Strobel, S. A. *Biochemistry* **2011**, *50*, 10491. (c) Kamerlin, S. C. L.; Chu, Z. T.; Warshel, A. *J. Org. Chem.* **2010**, *75*, 6391. (d) Zhang, Y.; Kua, J.; McCammon, J. A. *J. Am. Chem. Soc.* **2002**, *124*, 10572. (e) Childs, W.; Boxer, S. G. *Biochemistry* **2010**, *49*, 2725. (f) Whiting, A. K.; Peticolas, W. L. *Biochemistry* **1994**, *33*, 552. (g) Bryan, P.; Pantoliano, M. W.; Quill, S. G.; Hsiao, H. Y.; Poulos, T. *Proc. Natl. Acad. Sci. U.S.A.* **1986**, *83*, 3743.

(3) (a) Richter, F.; Blomberg, R.; Khare, S. D.; Kiss, G.; Kuzin, A. P.; Smith, A. J. T.; Gallaher, J.; Pianowski, Z.; Helgeson, R. C.; Grjasnow, A.; Xiao, R.; Seetharaman, J.; Su, M.; Vorobiev, S.; Lew, S.; Forouhar, F.; Kornhaber, G. J.; Hunt, J. F.; Montelione, G. T.; Tong, L.; Houk, K. N.; Hilvert, D.; Baker, D. *J. Am. Chem. Soc.* **2012**, *134*, 16197. (b) Beletskiy, E. V.; Schmidt, J.; Wang, X.-B.; Kass, S. R. *J. Am. Chem. Soc.* **2012**, *134*, 18534.

(4) (a) Desiraju, G. R. *Chem. Commun.* **2005**, 2995. (b) Desiraju, G. R.; Steiner, T. *The Weak Hydrogen Bond in Structural Chemistry and Biology*; Oxford University Press: Oxford, 1999.

(5) (a) Taylor, R.; Kennard, O. *J. Am. Chem. Soc.* **1982**, *104*, 5063. (b) Desiraju, G. R. *Acc. Chem. Res.* **1991**, *24*, 290. (c) Steiner, T. *Cryst. Rev.* **1996**, *6*, 1.

(6) (a) Derewenda, Z. S.; Lee, L.; Derewenda, U. *J. Mol. Biol.* **1995**, *252*, 248. (b) Wahl, M. C.; Sundaralingam, M. *Trends Biochem. Sci.* **1997**, *22*, 97. (c) Weiss, M. S.; Brandl, M.; Sühnel, J.; Pal, D.; Hilgenfeld, R. *Trends Biochem. Sci.* **2001**, *26*, 521. (d) Jiang, L.; Lai, L. *J. Biol. Chem.* **2002**, *277*, 37732.

(7) (a) Scheiner, T.; Kar, T. *J. Phys. Chem. A* **2008**, *112*, 11854. (b) Castellano, R. K. *Curr. Org. Chem.* **2004**, *8*, 845. (c) Koch, U.; Popelier, P. L. A. *J. Phys. Chem.* **1995**, *99*, 9747. (d) Steiner, T.; Desiraju, G. R. *Chem. Commun.* **1998**, 891.

(8) Jones, C. R.; Baruah, P. K.; Thompson, A. L.; Scheiner, S.; Smith, M. D. *J. Am. Chem. Soc.* **2012**, *134*, 12064.

(9) Houk, K. N.; Menzer, S.; Newton, S. P.; Raymo, F. M.; Stoddart, J. F.; Williams, D. J. *J. Am. Chem. Soc.* **1999**, *121*, 1479.
(10) Sato, K.; Okabe, Y.; Onitake, T.; Yamaguchi, M.; Arai, S.; Yamagishi, T. *Supramol. Chem.* **2011**, *23*, 249.
(11) (a) Lippert, K. M.; Hof, K.; Gerbig, D.; Ley, D.; Hausmann, H.; Guenther, S.; Schreiner, P. R. *Eur. J. Org. Chem.* **2012**, 5919. (b) Zhang, Z.; Lippert, K. M.; Hausmann, H.; Kotke, M.; Schreiner, P. R. *J. Org. Chem.* **2011**, *76*, 9764. (c) Kotke, M.; Schreiner, P. R. *Synthesis* **2007**, *5*, 779.
(12) (a) Chen, Y.; McDaid, P.; Deng, L. *Chem. Rev.* **2003**, *103*, 2965. (b) de Villegas, M. D. D.; Galvez, J. A.; Etayo, P.; Badorrey, R.; Lopez-Ram-de-Viu, P. *Chem. Soc. Rev.* **2011**, *40*, 5564. (c) Rodriguez-Docampo, Z.; Connon, S. J. *ChemCatChem* **2012**, *4*, 151. (d) Atodiresei, L.; Schiffers, I.; Bolm, C. *Chem. Rev.* **2007**, *1907*, 5683.
(13) (a) Bolm, C.; Gerlach, A.; Dinter, C. L. *Synlett* **1999**, 195. (b) Bolm, C.; Schiffers, I.; Dinter, C. L.; Gerlach, A. *J. Org. Chem.* **2000**, *65*, 6984. (c) Bolm, C.; Schiffers, I.; Atodireseim, I.; Hackenberger, C. P. R. *Tetrahedron: Asymmetry* **2003**, *14*, 3455.
(14) (a) Chen, Y.; Tian, S.-K.; Deng, L. *J. Am. Chem. Soc.* **2000**, *122*, 9542. (b) Li, H.; Liu, X.; Wu, F.; Tang, L.; Deng, L. *Proc. Natl. Acad. Sci. U.S.A.* **2010**, *107*, 20625.
(15) (a) Hiratake, J.; Yamamoto, Y.; Oda, J. *J. Chem. Soc., Chem. Commun.* **1985**, 1717. (b) Dedeoglu, B.; Catak, S.; Houk, K. N.; Aviyente, V. *ChemCatChem* **2010**, *2*, 1122. (c) Balzano, F.; Jumde, R. P.; Mandoli, A.; Masi, S.; Pini, D.; Uccello-Barretta, G. *Chirality* **2011**, *23*, 784.
(16) (a) Oh, S. H.; Rho, H. S.; Lee, J. W.; Lee, J. E.; Youk, S. H.; Chin, J.; Song, C. E. *Angew. Chem., Int. Ed.* **2008**, *47*, 7872. (b) Rho, H. S.; Oh, S. H.; Lee, J. W.; Lee, J. Y.; Chin, J.; Song, C. E. *Chem. Commun.* **2008**, 1208.
(17) (a) Jacobsen, E. N.; Marko, I.; Mungall, W. S.; Schroeder, G.; Sharpless, K. B. *J. Am. Chem. Soc.* **1988**, *110*, 1968. (b) Kolb, H. C.; Van Nieuwenhze, M. S.; Sharpless, K. B. *Chem. Rev.* **1994**, *94*, 2483.
(18) (a) Dijkstra, G. D. H.; Kellogg, R. M.; Wynberg, H.; Svendsen, J. S.; Marko, I.; Sharpless, K. B. *J. Am. Chem. Soc.* **1989**, *111*, 8069. (b) Dijkstra, G. D. H.; Kellogg, R. M.; Wynberg, H. *J. Org. Chem.* **1990**, *55*, 6121.
(19) (a) Li, H.; Wang, Y.; Tang, L.; Deng, L. *J. Am. Chem. Soc.* **2004**, *126*, 9906. (b) Wang, B.; Wu, F.; Wang, Y.; Liu, X.; Deng, L. *J. Am. Chem. Soc.* **2007**, *129*, 768.
(20) (a) Wang, Y.; Li, H.; Wang, Y.-Q.; Liu, Y.; Foxman, B. M.; Deng, L. *J. Am. Chem. Soc.* **2007**, *129*, 6364. (b) Shen, J.; Tan, C.-H. *Org. Biomol. Chem.* **2008**, *6*, 3229. (c) Singh, R. P.; Bartelson, K.; Wang, Y.; Su, H.; Lu, X.; Deng, L. *J. Am. Chem. Soc.* **2008**, *130*, 2422.
(21) Li, M.-Q.; Zhang, J.-X.; Huang, X.-F.; Wu, B.; Liu, Z.-M.; Chen, J.; Li, X.-D.; Wang, X.-W. *Eur. J. Org. Chem.* **2011**, 5237.
(22) (a) Zhao, Y.; Truhlar, D. G. *Theor. Chem. Acc.* **2008**, *120*, 215. (b) Zhao, Y.; Truhlar, D. G. *Acc. Chem. Res.* **2008**, *41*, 157.
(23) Cheong, P. H. Y.; Legault, C. Y.; M. Um, J. M.; Celebi-Olcum, N.; Houk, K. N. *Chem. Rev.* **2011**, *111*, 5042.
(24) (a) Jiang, Z.; Yang, H.; Han, X.; Luo, J.; Wong, M. W.; Lu, Y. *Org. Biomol. Chem.* **2010**, *8*, 1368. (b) Yang, H.; Wong, M. W. *J. Org. Chem.* **2011**, *76*, 7399. (c) Yang, H.; Wong, M. W. *Org. Biomol. Chem.* **2012**, *10*, 3229.
(25) (a) Cho, B.; Tan, C.-H.; Wong, M. W. *J. Org. Chem.* **2012**, *77*, 6553. (b) Cho, B.; Tan, C.-H.; Wong, M. W. *Org. Biomol. Chem.* **2011**, *9*, 4550.
(26) Marenich, A. V.; Cramer, C. J.; Truhlar, D. G. *J. Phys. Chem. B* **2009**, *113*, 6378.
(27) Reed, A. E.; Curtiss, L. A.; Weinhold, F. *Chem. Rev.* **1988**, *88*, 899.
(28) Bader, R. F. W. *Atoms in Molecules—A Quantum Theory*; Oxford Science Publications: Oxford, 1990.
(29) Popelier, P. L. A.; Bone, G. A. *MORPHY98*; UMIST: Manchester, 1998.
(30) Boys, S. F.; Bernardi, F. *Mol. Phys.* **1970**, *19*, 553.
(31) Frisch, M. J.; et al. *Gaussian 09*, Revision A.02; Gaussian, Inc.: Wallingford, CT, 2009.
(32) (a) Braje, W. M.; Holzgrefe, J.; Wartchow, R.; Hoffmann, H. M. R. *Angew. Chem., Int. Ed.* **2000**, *39*, 2085. (b) Kumaradhas, P.; Kalyanam, N.; Nirmala, K. A. *Cryst. Res. Technol.* **2001**, *36*, 1435. (c) Ishimaru, T.; Shibata, N.; Horikawa, T.; Yasuda, N.; Nakamura, S.; Toru, T.; Shiro, M. *Angew. Chem., Int. Ed.* **2008**, *47*, 4157. (d) Harding, M.; Bodkin, J. A.; Issa, F.; Hutton, C. A.; Willis, A. C.; McLeod, M. D. *Tetrahedron* **2009**, *65*, 831.
(33) (a) Chopra, D. *J. Phys. Chem. A* **2012**, *116*, 9791. (b) Ran, J.; Wong, M. W. *Aust. J. Chem.* **2009**, *62*, 1062. (c) Wojtulewski, S.; Grabowski, S. J. *Chem. Phys.* **2005**, *309*, 183.
(34) Meyer, V. R.; Rais, M. *Chirality* **1989**, *1*, 167.
(35) (a) Corey, E. J.; Noe, M. C. *J. Am. Chem. Soc.* **1993**, *115*, 12579. (b) Corey, E. J.; Noe, M. C.; Sarshar, S. *Tetrahedron Lett.* **1994**, *35*, 2861. (c) Corey, E. J.; Noe, M. C. *J. Am. Chem. Soc.* **1996**, *118*, 319. (d) Corey, E. J.; Noe, M. C. *J. Am. Chem. Soc.* **1996**, *118*, 11038.
(36) Davies, D. T. *Aromatic Heterocyclic Chemistry*; Oxford University Press: Oxford, 1992.
(37) (a) Cook, T. C.; Andrus, M. B.; Ess, D. H. *Org. Lett.* **2012**, *14*, 5836. (b) Corey, E. J.; Xu, F.; Noe, M. C. *J. Am. Chem. Soc.* **1997**, *119*, 12414. (c) Lygo, B.; G. Wainwright, P. G. *Tetrahedron Lett.* **1997**, *38*, 8595. (d) Lygo, B.; Andrews, B. I. *Acc. Chem. Res.* **2004**, *37*, 518. (e) Cannizzaro, C. E.; Houk, K. N. *J. Am. Chem. Soc.* **2002**, *124*, 7163. (f) Cannizzaro, C. E.; Strassner, T.; Houk, K. N. *J. Am. Chem. Soc.* **2001**, *123*, 2668. (g) Gomez-Bengoa, E.; Linden, A.; López, R.; Múgica-Mendiola, I.; Oiarbide, M.; Palomo, C. *J. Am. Chem. Soc.* **2008**, *130*, 7955.
(38) (a) Corey, E. J.; Lee, T. W. *Chem. Commun.* **2001**, 1321. (b) Ishihara, K.; Yamamoto, H. *J. Am. Chem. Soc.* **1994**, *116*, 1561. (c) Seebach, D.; Beck, A. K.; Heckel, A. *Angew. Chem., Int. Ed.* **2001**, *40*, 92. (d) Minamikawa, H.; Hayakawa, S.; Yamada, T.; Iwasawa, N.; Narasaka, K. *Bull. Chem. Soc. Jpn.* **1988**, *61*, 4379. (e) Corey, E. J.; Barnes-Seeman, D.; Lee, T. W. *Tetrahedron Lett.* **1997**, *38*, 1699. (f) Wong, M. W. *J. Org. Chem.* **2005**, *70*, 5487.
(39) (a) Custelcean, R.; Remy, P. *Cryst. Growth Des.* **2009**, *9*, 1985. (b) Ashley, E.; McGready, R.; Proux, S.; Nosten, F. *Travel Med. Infect. Dis.* **2006**, *4*, 159. (c) White, N. J. *Lancet Infect. Dis.* **2007**, *7*, 549. (d) Gao, D.; Cho, H.; Yang, W.; Pan, Y.; Yang, G.; Tai, H.-H.; Zhan, C.-G. *Angew. Chem., Int. Ed.* **2005**, *45*, 653. (e) Tamada, T.; Kinoshita, T.; Kurihara, K.; Adachi, M.; Ohhara, T.; Imai, K.; Kuroki, R.; Tada, T. *J. Am. Chem. Soc.* **2009**, *131*, 11033. (f) Zhang, Z.; Schreiner, P. R. *Chem. Soc. Rev.* **2009**, *38*, 1187. (g) Simon, L.; Muniz, F. M.; Saez, S.; Raposo, C.; Moran, J. R. *Eur. J. Org. Chem.* **2007**, *29*, 4821. (h) Veljkovic, D. Z.; Janjić, G. V.; Zaric, S. D. *CrystEngComm* **2011**, *13*, 5005. (i) Thomas, S. P.; Pavan, M. S.; Guru Row, T. N. *Cryst. Growth Des.* **2012**, *12*, 6083. (j) Kang, J.; Lee, H. G.; Han, Y.; Hwang, I. H.; Kim, C.; Cho, S. J. *Supramol. Chem.* **2012**, *24*, 738. (k) Horowitz, S.; Trievel, R. C. *J. Biol. Chem.* **2012**, *287*, 41576. (l) Mayo, P.; Orlova, G.; Goddard, J. D.; Tam, W. *J. Org. Chem.* **2001**, *66*, 5182.